PHASE TRANSFORMATION

Microscopic mechanisms of equilibrium melting of a solid

Amit Samanta,[1,2]* Mark E. Tuckerman,[3,4,5]* Tang-Qing Yu,[6] Weinan E[7,8]*

The melting of a solid, like other first-order phase transitions, exhibits an intrinsic time-scale disparity: The time spent by the system in metastable states is orders of magnitude longer than the transition times between the states. Using rare-event sampling techniques, we find that melting of representative solids—here, copper and aluminum—occurs via multiple, competing pathways involving the formation and migration of point defects or dislocations. Each path is characterized by multiple barrier-crossing events arising from multiple metastable states within the solid basin. At temperatures approaching superheating, melting becomes a single barrier-crossing process, and at the limit of superheating, the melting mechanism is driven by a vibrational instability. Our findings reveal the importance of nonlocal behavior, suggesting a revision of the perspective of classical nucleation theory.

Theoretical work on the melting of a solid dates back to Lindemann, who in 1910 envisioned the melting transition as a vibrational instability (*1*). In 1939, Born postulated the macroscopic instability criteria of a solid in terms of the elastic constants (*2*–*4*). Most other theoretical models are centered around the role of defects, including point defects such as vacancies and interstitials and line defects such as dislocations, that proliferate in the solid close to the melting point (*5*–*8*).

Contrary to these melting theories, classical notions of homogeneous melting envision the formation of an initial liquid nucleus that is aided by thermal fluctuations without any preferential nucleating sites (*9*, *10*). Within the framework of the classical nucleation theory (CNT), the radius r of the liquid nucleus serves as a reaction coordinate, and the Gibbs free energy $\Delta G(r)$ is a balance between the free energy gained in forming a liquid nucleus of volume $4\pi r^3/3$ and the work needed to create an interface between the solid and such a nucleus

$$\Delta G(r) = \frac{4}{3}\pi r^3 \rho \Delta\mu + 4\pi r^2 \gamma_s \qquad (1)$$

Here, $\Delta\mu = \mu_l - \mu_s < 0$ is the chemical potential difference between the liquid and solid phases, ρ is the liquid density, $4\pi r^2$ is the surface area of the nucleus, and γ_s is its surface tension. The critical nucleus size $r^* = -2\gamma_s/(\rho\Delta\mu)$ maximizes this free energy [$\Delta G(r^*) = 16\pi\gamma_s^3/3(\rho\Delta\mu)^2$] (*11*) and determines the length scale beyond which growth of the cluster becomes favorable. At the solid-liquid coexistence point, $\Delta\mu = 0$, and the theory predicts an infinite free-energy barrier and corresponding suppression of the nucleation rate. This picture involves numerous simplifying assumptions and fails to account for the potentially important role of defects, dislocations, and multiple barriers along potential melting paths (*11*).

Close to the coexistence point, the melting of a solid involves activation from a metastable local minimum. Consequently, a theoretical analysis of the melting mechanisms using standard atomistic simulation methods is not feasible because melting is a rare barrier-crossing event with mean first passage time many orders of magnitude greater than the vibrational frequency of atoms. State-of-the-art rare-event sampling techniques now render possible the computational study of equilibrium melting and the extraction of dominant pathways and free energetics. We used adiabatic free-energy dynamics (AFED) (*12*) together with the string method (*13*, *14*) in order to explore the multidimensional free-energy surface (FES) efficiently and to construct a microscopic picture of the melting process for two commonly studied prototypical systems: copper (Cu) and aluminum (Al) (*15*, *16*).

We began by analyzing the equilibrium melting process using as collective variables the volume (V) of the system and the two Steinhardt order parameters Q_4 and Q_6 (*17*); this combination captures the positional and orientational ordering. In Fig. 1, A and B, we show a projection of the Gibbs FES onto the V-Q_4 subspace for Cu at 1350 K, close to the melting point of 1358 K, and 1 atm pressure. Contrary to the simple picture from CNT of a smooth FES possessing metastable solid and liquid basins separated by an index-1 saddle point, the FES obtained here has multiple locally stable states characterized by different defects—primarily vacancy-interstitial pairs, dislocations, and interstitial clusters—and the free-energy barriers separating these states range over multiple energy scales. The FES for Al (fig. S1), close to the melting point of 933 K, exhibits a similar structure. How vacancy-interstitial pairs can form, diffuse, cluster, and annihilate is illustrated in Fig. 1C.

The existence of a multitude of metastable states suggests that there exists an ensemble of multiple competing transition pathways. One such melting channel and the associated free energy profile are shown in Fig. 2A. Along this path, as the system moves out of the solid basin, the volume of the solid and the number of vacancy and interstitial pairs increases. Thus, this particular melting pathway proceeds via the formation of point defects, which is entropically favorable but energetically costly. The competition between entropic and enthalpic contributions causes the free energy to reach a maximum value (Fig. 2A, "S2") at a certain defect concentration. After the saddle S2, the system lowers its free energy by forming defect clusters at the expense of isolated defects. Cluster formation is enabled via the defect kinetics. In both Cu and Al, diffusion barriers of interstitial defects are quite small (0.09 and 0.13 eV, respectively); barriers for vacancy diffusion are somewhat larger (0.70 and 0.65 eV, respectively). Previously, Couchman and Reynolds had conjectured that a relationship exists between the melting point and vacancy concentration, thus suggesting a direct role for vacancy diffusion in the melting process (*18*). At 1350 K in Cu, these defects are mobile and diffuse over long distances in the solid. Occasionally, some of these interstitial and vacancy migration paths meet, and defect clusters can form. Inside these defect clusters, there is a notable loss of crystalline order (the local Steinhardt parameter $q_6 \sim 0.1$), which coincides with an enhanced diffusivity of atoms inside the cluster. After S2, the system moves to a shallow metastable state, and the defect cluster evolves into a liquid nucleus, the existence of which during melting also constitutes a deviation from the CNT.

As the system moves out of the metastable state toward the saddle S1 (fig. S3), the size of the liquid nucleus increases. This process is sometimes observed to be aided by the coalescence of a few smaller liquid nuclei. A test of the system size scaling of the free-energy barrier (fig. S3E) reveals that the S1 barrier scales roughly as $N^{2/3}$. After the liquid nucleus attains a critical size, the free energy along the path decreases. This corresponds to the second important bottleneck, with a barrier of ~125 eV relative to the solid basin. From here, the liquid nucleus simply increases in size until the entire system transforms to the liquid state.

Our enhanced sampling calculations suggest the existence of a melting path along which dislocation activity aids the formation of an initial liquid nucleus. The corresponding free-energy profile and key saddle structures are shown in

[1]Condensed Matter and Materials Division, Lawrence Livermore National Laboratory, Livermore, CA 94550 USA. [2]Program in Applied and Computational Mathematics, Princeton University, Princeton, NJ 08544, USA. [3]Department of Chemistry, New York University (NYU), New York, NY 10003, USA. [4]Courant Institute of Mathematical Sciences, NYU, New York, NY 10012, USA. [5]NYU–East China Normal University Center for Computational Chemistry at NYU Shanghai, Shanghai 200062, China. [6]Courant Institute of Mathematical Sciences, NYU, New York, NY 10012, USA. [7]Beijing International Center for Mathematical Research and School of Mathematical Sciences, Peking University, Beijing, China. [8]Department of Mathematics and Program in Applied and Computational Mathematics, Princeton University, Princeton, NJ 08544, USA.
*Corresponding author. E-mail: asamanta@math.princeton.edu (A.S.); weinan@math.princeton.edu (W.E.); mark.tuckerman@nyu.edu (M.E.T.)

Fig. 2B. Along this path, we first observe the formation of defect clusters from point defects followed by the heterogeneous nucleation of dislocations from the defect clusters. The dislocation density increases as the system moves toward the saddle S1, and the first liquid embryo is formed heterogeneously from these dislocations. This process of initiating melting from dislocations is reminiscent of recent observations of heterogeneous nucleation in colloidal systems (*19*) and embedded lead (Pb) nanoparticles in an Al matrix (*20*) and differs considerably from the notion of proliferation of dislocations (*5*, *7*).

From our analysis of the escape pathways from the solid basin, we conclude that melting has a high probability of being coupled to defect activity. Nevertheless, motivated by recent reports of melting without the aid of defects (*21*), we were inspired to ask whether it is possible for melting to occur in this manner. By calculating Voronoi volumes associated with each of the atoms, we are able to show that close to the melting point, the free volume associated with vacancies is spatially delocalized, and it is difficult to identify individual defects. Previous experiments have shown that on-the-fly determination of defects at high temperatures is nontrivial (*22*). Furthermore, under equilibrium conditions, the possibility that Cu at 1350 K is defect-free seems remote because of the presence of nearly degenerate defect states, with transition barriers on the order of 1 to 4 eV. Nevertheless, we explored the possibility of a melting pathway connecting the defect-free solid minimum and the liquid basin that does not pass through the defect states. On the FES, a possible pathway for melting without the aid of defects has a notably higher free-energy barrier (~150 eV) than the barriers along the defect-mediated melting pathways. Along such a defect-free path, the formation of the initial liquid nucleus is correlated with thermal fluctuations and is not aided by any stable defects. However, if this path is allowed to relax in path space, it eventually converges to one of the two defect-mediated melting pathways.

Temperature plays an important role in determining the characteristics of the FES. Thus, we also sought to compare equilibrium melting to melting of a superheated solid. As the system is superheated beyond the melting point, the liquid basin engulfs larger portions of the FES, and the metastable state without defects vanishes (Fig. 2E). This change in the FES affects the melting mechanisms: Compared with the FES at 1350 K in Cu, at 1550 K (and at 1200 K for Al) there are fewer locally stable states present inside the solid basin, and there is only one important bottleneck for melting—namely, the barrier to escape the solid basin. This barrier has a substantial entropic contribution (fig. S4). The absence of a metastable state without defects indicates that melting at these superheated conditions always originates from a solid with preexisting point defects or defect clusters.

With further increase in temperature, the melting barrier along the minimum free-energy path vanishes at ~1600 K in Cu and ~1275 K in Al. Above these temperatures, atoms execute large-amplitude vibrations about their equilibrium positions, and the solid-to-liquid transition is a consequence of an instability (Fig. 2C, inset, and fig. S5). The crucial role of the vibrational amplitude in this process is realized only by separating the diffusive motions of the atoms from their vibrational motions. This mechanism is reminiscent of Lindemann's vibrational instability (*1*) and is in agreement with recent experimental observations of melting in superheated aluminum (*23*). The fact that Lindemann's criterion corresponds to an instability of the solid and not to equilibrium melting leads to an overestimation of the melting point. This is relevant because Lindemann's criterion is still commonly used to determine the melting point of a solid (*24*–*26*).

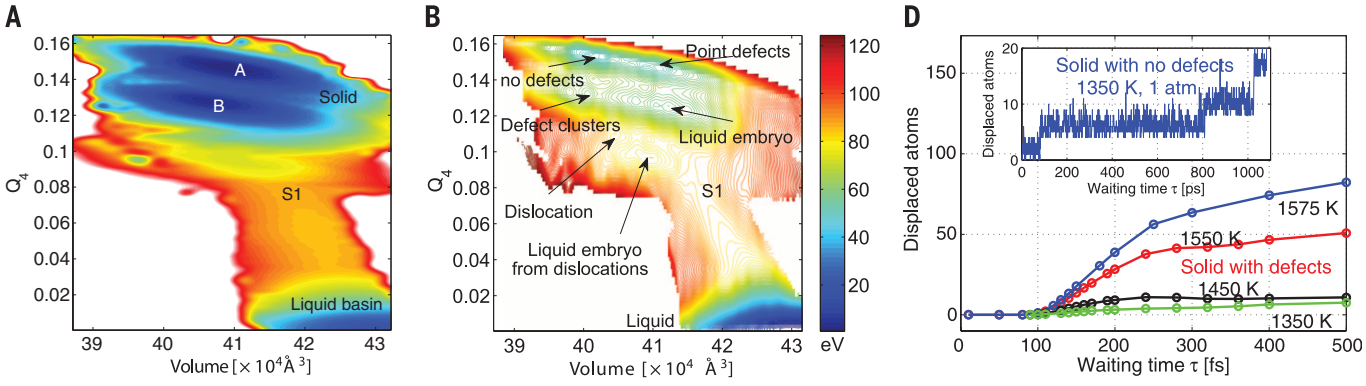

Fig. 1. The FES of a solid shows multiscale characteristics and is sensitive to temperature. (**A** and **B**) The FESs at 1350 K, 1 atm for Cu. The solid basin contains two valleys [(A), "A" and "B"] separated by a shallow ridge. Valley A contains local minima pertaining to the solid with or without point defects, whereas Valley B contains local minima pertaining mainly to defect clusters. Within valley A, atomic motions in the state without defects are highly correlated and have a waiting time of ~300 ps [analyzed by calculating the number of atoms displaced more than nearest-neighbor spacings, (**D**), inset], whereas point defect–related diffusive motions of atoms have a waiting time of ~0.10 ps [(D) and fig. S2]. Inside valley B, as the volume of the system increases, the defect cluster develops liquidlike characteristics. (**C**) A time evolution of defects in the solid basin. The dominant atomic processes are vacancy-interstitial formation, vacancy diffusion (indicated with blue arrows), interstitial diffusion (black arrows), interstitial cluster formation, and vacancy-interstitial annihilation (red double-ended arrow). Processes such as vacancy-interstitial pair formation and cluster formation are circled in red.

Theories such as CNT and that suggested by the present study address homogeneous melting in the bulk. The system-size scaling dependence of the associated free-energy barrier, however, indicates that as N grows, melting is more likely to be initiated from regions that break the translational and orientational order of the bulk solid. These include defect clusters, voids, grain boundaries, and dislocations, all of which increase the energy of a solid and lead to heterogeneous melting. We sought to investigate this case by initiating trajectories from preexisting dislocations and from grain boundaries obtained by rapidly cooling the liquid [(*17*), section XII, fig. S6]. In both cases, the resulting metastable states lie closer to the saddle S1 on the FES, resulting in a decrease in the melting barrier. As shown in Fig. 2D, melting in a solid with grain boundaries is initiated at these boundaries, and the barrier can be as low as 6 eV at the melting point (fig. S7). The atoms in the grain boundaries are fluid-like, and hence, melting occurs via gradual growth of these liquid-like regions. In a solid with multiple dislocations, the elastic interactions between the dislocations can decrease the melting barrier by as much as a factor of six below the barrier for melting of a Cu sample without preexisting defects.

The sensitivity of the free-energy surface to temperature is shown in Fig. 2C. There exist three different melting regimes: (i) Close to the melting point [temperature (T) < 1525 K for Cu, T < 1200 K for Al], the transition occurs via multiple barrier crossings, and elastic interactions play a dominant role in determining the melting mechanisms. (ii) At superheated temperatures (1525 to 1590 K for Cu, 1200 to 1265 K for Al), the solid-to-liquid transition is a single barrier-crossing event, and the barrier contains enthalpic as well as entropic contributions. (iii) At the limit of instability, melting is initiated by the propagation of large vibrations of the atoms in a short span of time across the crystal. This large variation in the underlying melting mechanisms suggests a strong coupling between the orientational order, density, and temperature: At a given temperature, how Q_6 and Q_4 change with V determines the structure of defects present in the solid, locations of the saddle points, and the basins of attraction.

Notwithstanding the above differences in the melting mechanisms, we find that melting is aided by mobile defects both at the thermodynamic melting point and at conditions of superheating. In both of these states, defects constitute less than 1/1000 of the total lattice sites. Consequently, melting and lattice instabilities are not triggered by the proliferation of defects (*6*, *27*, *28*), which contrasts with theories based on the assertion that "melting is correlated with the achievement of a critical vacancy concentration" (*29*). Further, our enhanced sampling calculations reveal that the size of a liquid nucleus does not change smoothly along the minimum free-energy pathway.

It is clear that multiple, competing pathways and multiple barrier-crossing events along each path are crucial for the formation of the initial liquid embryo and constitute a qualitative departure from the simplifying assumptions of CNT. An important element that is clearly missing in the ΔG of CNT is the contribution from the strain energy. Along the dislocation-mediated melting pathway (Fig. 2B), the liquid nucleus is formed preferentially on the dislocations via a decrease in the strain energy associated with the dislocations. The change in free energy can be expressed as $\Delta G(r) = -\alpha r \log r/r_o + \Delta\mu 4\pi r^3/3 + 4\pi r^2\gamma_s$, where $\alpha = Gb^2/4\pi(1-\nu)$, r_o is a constant, b is the Burgers vector, ν is Poisson's ratio, and $-\alpha r \log r/r_o$ is the decrease in the elastic energy of the dislocation owing to the formation of the liquid nucleus (*30*). At the melting point, $\Delta\mu = 0$; hence, the critical radius of the liquid nucleus is $r^* \sim Gb^2/32\pi^2\,\gamma_s(1-\nu)$. Similarly, formation of dislocations from point defects and defect clusters involves a competition between the elastic energy of dislocation and the interaction energy between the dislocation and the defects, likely requiring the addition of nonlocal energy terms in any mean-field type of description of melting. This physical interplay of processes with multiple length and time scales indicates that melting of a solid cannot be viewed through the simple lens of CNT but should be regarded as a complex "multiscale" phenomenon.

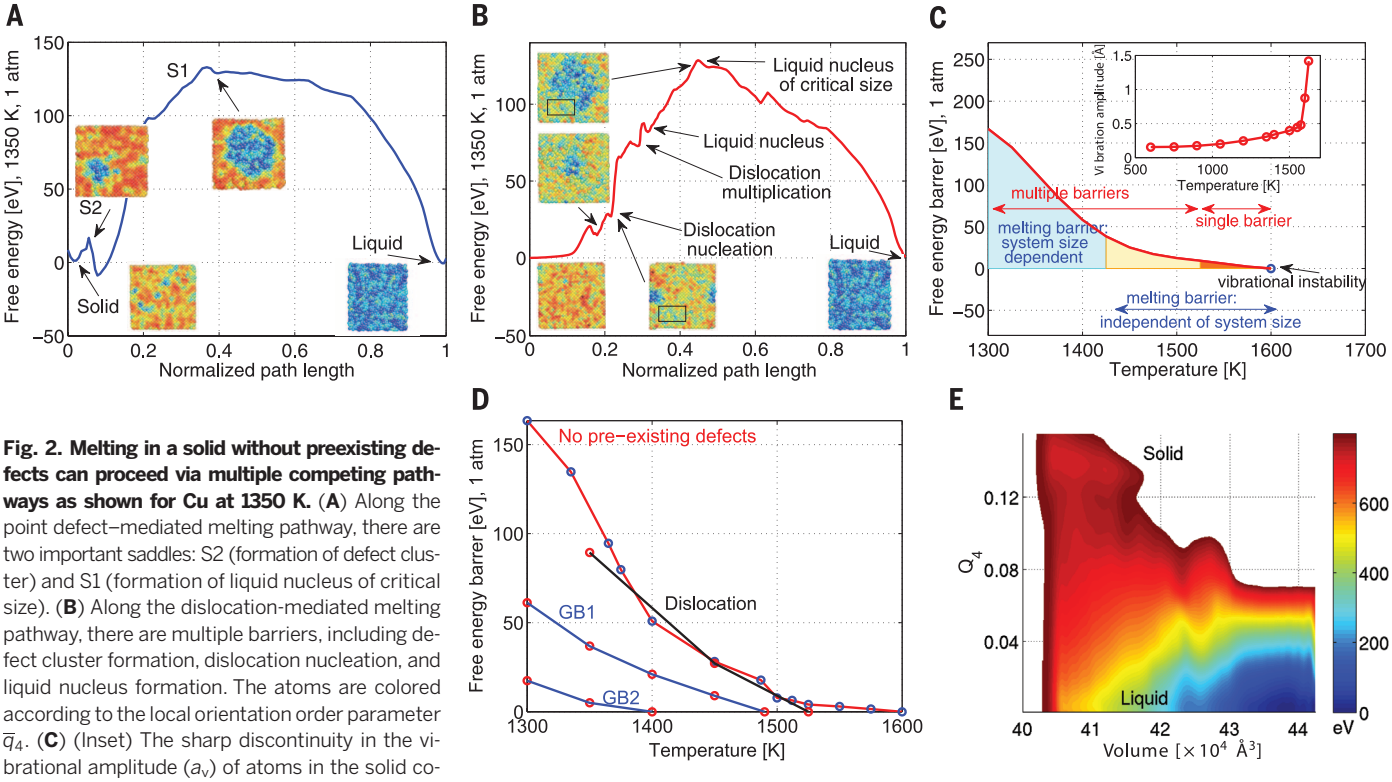

Fig. 2. Melting in a solid without preexisting defects can proceed via multiple competing pathways as shown for Cu at 1350 K. (**A**) Along the point defect–mediated melting pathway, there are two important saddles: S2 (formation of defect cluster) and S1 (formation of liquid nucleus of critical size). (**B**) Along the dislocation-mediated melting pathway, there are multiple barriers, including defect cluster formation, dislocation nucleation, and liquid nucleus formation. The atoms are colored according to the local orientation order parameter $\bar{q}_4$. (**C**) (Inset) The sharp discontinuity in the vibrational amplitude (a_v) of atoms in the solid coincides with the vanishing of the free-energy barrier. a_v is extracted from the root-mean-squared-displacement (RMSD) after subtracting the diffusion contributions, and hence, the sharp discontinuity observed in a_v is not observed in the usual RMSD profiles [for example, figure 2 in (*25*)]. (**D**) The effect of grain boundaries and dislocations on the melting barriers. The solid in GB1 has only two grains, whereas GB2 has about four grains. (**E**) FES at 1550 K for Cu, illustrating that melting is a single barrier-crossing event that involves enthalpic as well as entropic barriers at superheated conditions.

REFERENCES AND NOTES

1. F. A. Lindemann, *Phys. Z.* **11**, 609 (1910).
2. M. Born, *J. Chem. Phys.* **7**, 591 (1939).
3. N. F. Mott, *Nature* **145**, 801–802 (1940).
4. J. L. Tallon, *Nature* **299**, 188 (1982).
5. D. Kuhlmann-Wilsdorf, *Phys. Rev.* **140**, A1599–A1610 (1965).
6. T. Gorecki, *Z. Metallkunde Mat. Res. Adv. Tech.* **65**, 426 (1974).
7. L. Gómez, A. Dobry, Ch. Geuting, H. T. Diep, L. Burakovsky, *Phys. Rev. Lett.* **90**, 095701 (2003).
8. X. M. Bai, M. Li, *Phys. Rev. B* **77**, 134109 (2008).
9. M. Volmer, A. Weber, *Z. Phys. Chem.* **119**, 277 (1926).
10. R. Becker, W. Döring, *Ann. Phys.* **416**, 719–752 (1935).
11. R. P. Sear, *Int. Mater. Rev.* **57**, 328–356 (2012).
12. T. Q. Yu, M. E. Tuckerman, *Phys. Rev. Lett.* **107**, 015701 (2011).
13. W. E, W. Ren, E. Vanden-Eijnden, *J. Phys. Chem. B* **109**, 6688–6693 (2005).
14. L. Maragliano, A. Fischer, E. Vanden-Eijnden, G. Ciccotti, *J. Chem. Phys.* **125**, 024106 (2006).
15. R. Lynden-Bell, J. Van Duijneveldt, D. Frenkel, *Mol. Phys.* **80**, 801–814 (1993).
16. M. Forsblom, G. Grimvall, *Nat. Mater.* **4**, 388–390 (2005).
17. Materials and methods are available as supplementary materials on *Science* Online
18. P. R. Couchman, C. L. Reynolds Jr., *Philos. Mag.* **34**, 327–329 (1976).
19. A. M. Alsayed, M. F. Islam, J. Zhang, P. J. Collings, A. G. Yodh, *Science* **309**, 1207–1210 (2005).
20. H. Rösner, B. Freitag, G. Wilde, *Philos. Mag. Lett.* **87**, 341–347 (2007).
21. Z. Wang, F. Wang, Y. Peng, Z. Zheng, Y. Han, *Science* **338**, 87–90 (2012).
22. E. Fukushima, A. Ookawa, *J. Phys. Soc. Jpn.* **10**, 970–981 (1955).
23. B. J. Siwick, J. R. Dwyer, R. E. Jordan, R. J. D. Miller, *Science* **302**, 1382–1385 (2003).
24. J. J. Gilvarry, *Phys. Rev.* **102**, 308–316 (1956).
25. Z. H. Jin, P. Gumbsch, K. Lu, E. Ma, *Phys. Rev. Lett.* **87**, 055703 (2001).
26. K. Sokolowski-Tinten *et al.*, *Nature* **422**, 287–289 (2003).
27. R. M. J. Cotterill, J. U. Madsen, *Nature* **288**, 467–469 (1980).
28. H. J. Fecht, W. L. Johnson, *Nature* **334**, 50–51 (1988).
29. R. W. Cahn, *Nature* **334**, 17–18 (1988).
30. J. W. Cahn, *Acta Metall.* **5**, 169–172 (1957).

ACKNOWLEDGMENTS

Work by W.E and A.S. at Princeton was supported by the U.S. Department of Energy (DOE) (grant DE-SC0009248) and in Beijing by the National Natural Science Foundation of China (9130005). This work was partially performed under the auspices of DOE by Lawrence Livermore National Laboratory under contract DE-AC52-07NA27344. Work by M.E.T. was supported by NSF grant CHE-1301314.

SUPPLEMENTARY MATERIALS

www.sciencemag.org/content/346/6210/729/suppl/DC1
Materials and Methods
Figs. S1 to S7
References (*31*–*41*)

24 March 2014; accepted 10 October 2014
10.1126/science.1253810

EARLY UNIVERSE

On the origin of near-infrared extragalactic background light anisotropy

Michael Zemcov,[1,2] Joseph Smidt,[3,4] Toshiaki Arai,[5,6] James Bock,[1,2]* Asantha Cooray,[4] Yan Gong,[4] Min Gyu Kim,[7] Phillip Korngut,[2,1] Anson Lam,[8,1] Dae Hee Lee,[9] Toshio Matsumoto,[5,10] Shuji Matsuura,[5] Uk Won Nam,[9] Gael Roudier,[2] Kohji Tsumura,[11] Takehiko Wada[5]

Extragalactic background light (EBL) anisotropy traces variations in the total production of photons over cosmic history and may contain faint, extended components missed in galaxy point-source surveys. Infrared EBL fluctuations have been attributed to primordial galaxies and black holes at the epoch of reionization (EOR) or, alternately, intrahalo light (IHL) from stars tidally stripped from their parent galaxies at low redshift. We report new EBL anisotropy measurements from a specialized sounding rocket experiment at 1.1 and 1.6 micrometers. The observed fluctuations exceed the amplitude from known galaxy populations, are inconsistent with EOR galaxies and black holes, and are largely explained by IHL emission. The measured fluctuations are associated with an EBL intensity that is comparable to the background from known galaxies measured through number counts and therefore a substantial contribution to the energy contained in photons in the cosmos.

At near-infrared wavelengths, where the large zodiacal light foreground complicates absolute photometry measurements, the extragalactic background light (EBL) may be best accessed by anisotropy measurements. On large angular scales, fluctuations are produced by the clustering of galaxies, which is driven by the underlying distribution of dark matter. EBL anisotropy measurements can probe emission from epoch of reionization (EOR) galaxies (*1*–*3*) and direct-collapse black holes (*4*) that formed during the EOR before the universe was fully ionized by exploiting the distinctive Lyman cutoff feature in the rest-frame ultraviolet (UV), thus probing the UV luminosity density at high redshifts (*5*). However, large-scale fluctuations may also arise from the intrahalo light (IHL) created by stars stripped from their parent galaxies during tidal interactions (*6*) at redshift $z < 3$. A multiwavelength fluctuation analysis can distinguish among these scenarios and constrain the EOR star formation rate.

A search for such background components must carefully account for fluctuations produced by known galaxy populations. Linear galaxy clustering is an important contribution to fluctuations on scales much larger than galaxies themselves. On fine scales, the variation in the number of galaxies produces predominantly Poissonian fluctuations, with an amplitude that depends on the luminosity distribution. Anisotropy measurements suppress foreground galaxy fluctuations by masking known galaxies from an external catalog.

The first detections of infrared fluctuations in excess of the contribution from known galaxies with the Spitzer Space Telescope (*7*–*9*) were interpreted as arising from a population of faint first-light galaxies at $z > 7$. The Hubble Space Telescope was used at shorter wavelengths (*10*) to carry out a fluctuation study in a small deep field but did not report fluctuations in excess of known galaxy populations. Measurements with the AKARI satellite (*11*) show excess fluctuations with a blue spectrum rapidly rising from 4.1 μm to 2.4 μm. Fluctuation measurements in a large survey field (*6*) with Spitzer agreed with earlier measurements (*7*–*9*) but were instead interpreted as arising from tidally stripped stars at $z \sim 1$ to 3. Most recently, a partial correlation has been reported (*12*) between Spitzer and soft x-ray images, which Yue *et al.* (*4*) interpret as arising from direct-collapse black holes at $z > 12$.

We have developed and flown the specialized Cosmic Infrared Background Experiment [CIBER (*13*)], a rocket-borne instrument specifically designed to study the spatial and spectral properties of the EBL. The imaging instrument (*14*) measures fluctuations in $\Delta\lambda/\lambda = 0.5$ bands centered at 1.1 and 1.6 μm using two 11-cm telescopes each with a 2° by 2° field of view. Here, we report our analysis of data from two flights in 2010 and 2012.

The CIBER imager data are reduced from raw telemetered time streams, flat-field–corrected based

[1]Department of Physics, Mathematics, and Astronomy, California Institute of Technology, Pasadena, CA 91125, USA. [2]Jet Propulsion Laboratory (JPL), National Aeronautics and Space Administration (NASA), Pasadena, CA 91109, USA. [3]Theoretical Division, Los Alamos National Laboratory, Los Alamos, NM 87545, USA. [4]Department of Physics and Astronomy, University of California, Irvine, CA 92697, USA. [5]Department of Space Astronomy and Astrophysics, Institute of Space and Astronautical Science (ISAS), Japan Aerospace Exploration Agency (JAXA), Sagamihara, Kanagawa 252-5210, Japan. [6]Department of Physics, Graduate School of Science, The University of Tokyo, Tokyo 113-0033, Japan. [7]Department of Physics and Astronomy, Seoul National University, Seoul 151-742, Korea. [8]Department of Physics and Astronomy, University of California, Los Angeles, CA 90095, USA. [9]Korea Astronomy and Space Science Institute (KASI), Daejeon 305-348, Korea. [10]Institute of Astronomy and Astrophysics, Academia Sinica, Taipei 10617, Taiwan, Republic of China. [11]Frontier Research Institute for Interdisciplinary Science, Tohoku University, Sendai, Miyagi, 980-8578, Japan.
***Corresponding author. E-mail: jjb@astro.caltech.edu**